Schweizerischer Erdbebendienst
Service Sismologique Suisse
Servizio Sismico Svizzero
Swiss Seismological Service

ETH
Eidgenössische Technische Hochschule Zürich
Swiss Federal Institute of Technology Zurich

SITE CHARACTERIZATION REPORT

SMEIS: Meiringen (BE)

Dario Chieppa, Manuel Hobiger, Donat Fäh

Last Modification: 5th October, 2021

Schweizerischer Erdbebendienst (SED)
Service Sismologique Suisse
Servizio Sismico Svizzero
Servizi da Terratrembels Svizzer
ETH Zürich
Sonneggstrasse 5
8092 Zürich
Schweiz
dario.chieppa@sed.ethz.ch

Contents

Summary

Meiringen (BE) is a city located in central Switzerland in the valley of the Aare river. The place was chosen as site for the installation of a new station, called SMEIS, as part of the renewal project of the Swiss Strong Motion Network (SSMNet). In order to better assess the local subsurface, we performed a passive seismic array measurement around the location of the seismic station SMEIS. The horizontal-to-vertical spectral ratio (H/V) curves show one asymmetric peak between 1.3 and 1.6 Hz followed by a narrow trough at 2.2 Hz. The peak is interpreted as fundamental H/V peak (f_0) and shows a left flank less inclined than the right one. The Raydec curves show a secondary peak at about 13-15 Hz.

The inversion of the passive seismic array measurements allows the estimation of the velocity profiles down to 250 m. Using a profile with 5, 7 or 9 layers over the half-space, three main interfaces are distinguished at depths of about 1.5, 17 and 73 meters. The basement with S-wave velocity of about 1500 m/s is located at about 180 meters.

The V_{S30} value of the site is around 380 m/s, corresponding to soil class B in EC8 and C in SIA261. The theoretical shear-wave transfer functions from the retrieved V_S profiles predict an amplification function in good agreement with the empirical function recorded at station SMEIS.

1 Introduction

The station SMEIS is part of the Swiss Strong Motion Network (SSMNet). The station was installed on 6 August 2019 in the framework of the second phase of the Swiss Strong Motion Network (SSMNet) renewal project (Fig. 1). In order to better characterize the underground, to estimate the fundamental frequency of the site and the shear wave velocity profile, a passive array measurement was carried out on 30 September 2020.

The site is of interest for its location in a populated area in central Switzerland and for the possibility to improve the network coverage of central Switzerland. From a geological point of view, Meiringen is located on undifferentiated alluvial sediments of Holocene age overlying the Helvetic nappes.

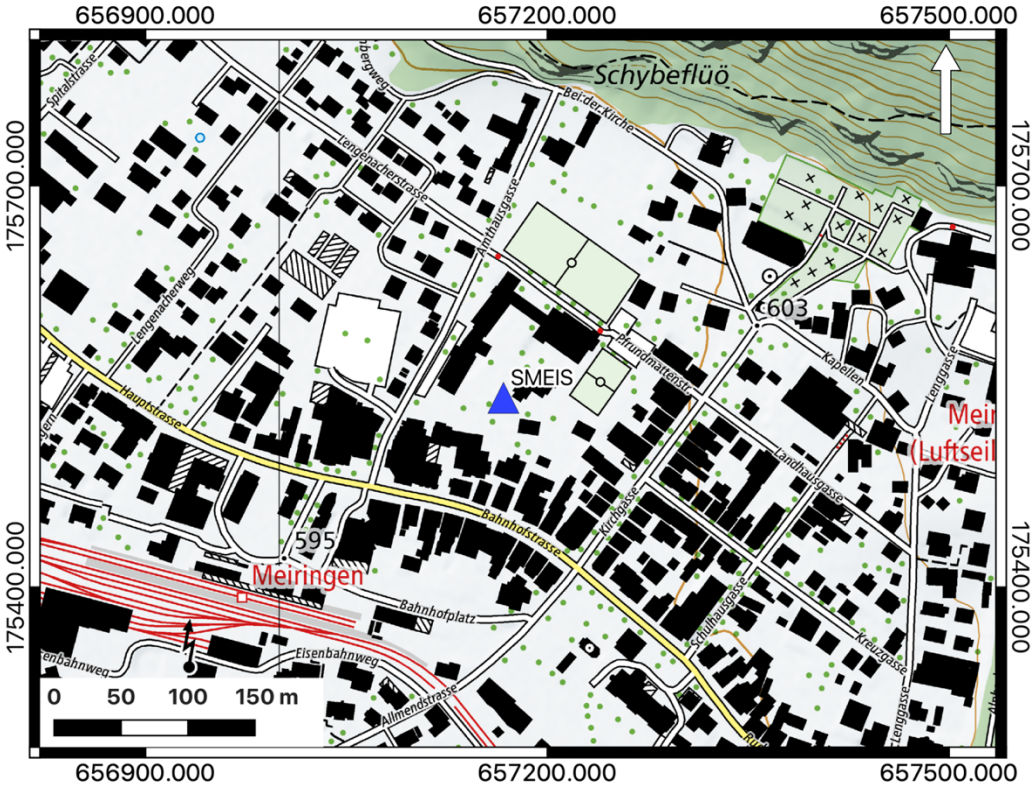

Figure 1: Map showing the location of the strong motion station (blue triangle) in Meiringen. Source: Federal Office of Topography.

2 Geological setting

A geological map of the surroundings of Meiringen is shown in Fig. 2. Red dots represent the location of the passive array measurement, the blue triangle the location of station SMEIS. One sensor is located on river gravels (Holocene), while the other fifteen and the seismic station SMEIS are located on undifferentiated alluvial sediments (Holocene). Towards north, outside of the study area, marls, claystones and sandstones of Middle Jurassic age were mapped.

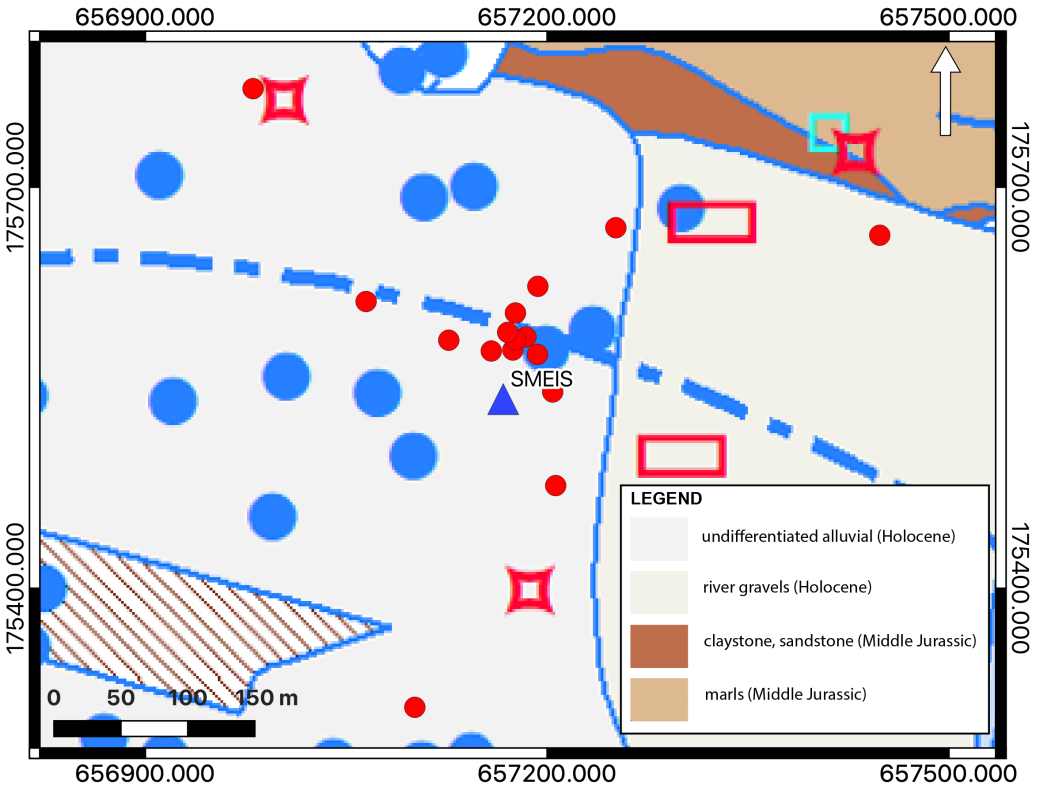

Figure 2: Geological map of the Meiringen area. The stations of the passive array recordings are indicated by red triangles, whereas the position of the strong-motion station SMEIS is shown by a blue triangle. Source: Federal Office of Topography.

3 Passive site characterization measurements

3.1 Data set

To characterize the underground structure around the seismic station, a passive seismic measurement and an additional H/V single point measurement (SMEIS1) at the location of station SMEIS were performed on 30 September 2020.

A single array of 16 stations was installed (Fig. 4). The stations were planned to be located on five rings of different radii around a central station. The three stations of each ring were planned to be rotated by 120 degrees one from the other. The radii of the rings are 8, 20, 50, 115 and 280 meters. The central array station (MEIS55) is located 50 m from SMEIS. Each ring, starting from the second, was rotated with respect to the previous ring by 30, 25, 42 and 32 degrees.

Each station consisted of a Lennartz 5s sensor connected to a Centaur digitizer, with the exception of four stations in the central part which had two sensors connected to the same digitizer. The station names of the array are composed of "MEIS" followed by a two-digit number between 42 and 49, 52 and 55, 64, 65, 72 and 75 (corresponding to the Centaur digitizer serial number for numbers lower than 60 plus 20 to distinguish the use of the second channel). The array recording time was 189 minutes (11340 s). The station locations were measured by a differential GPS system (Leica Viva GS10) which was set up to measure with a precision better than 5 cm. This precision was met at most stations with two exceptions. For MEIS47, the precision was only 11.8 cm. MEIS53 was located in a court surrounded by relatively high walls and had therefore a bad GPS precision of only 1.30 m. Its location was therefore derived from the aerial image at map.geo.admin.ch with a better precision.

Figure 3: Seismic station installation example for the measurements in Meiringen.

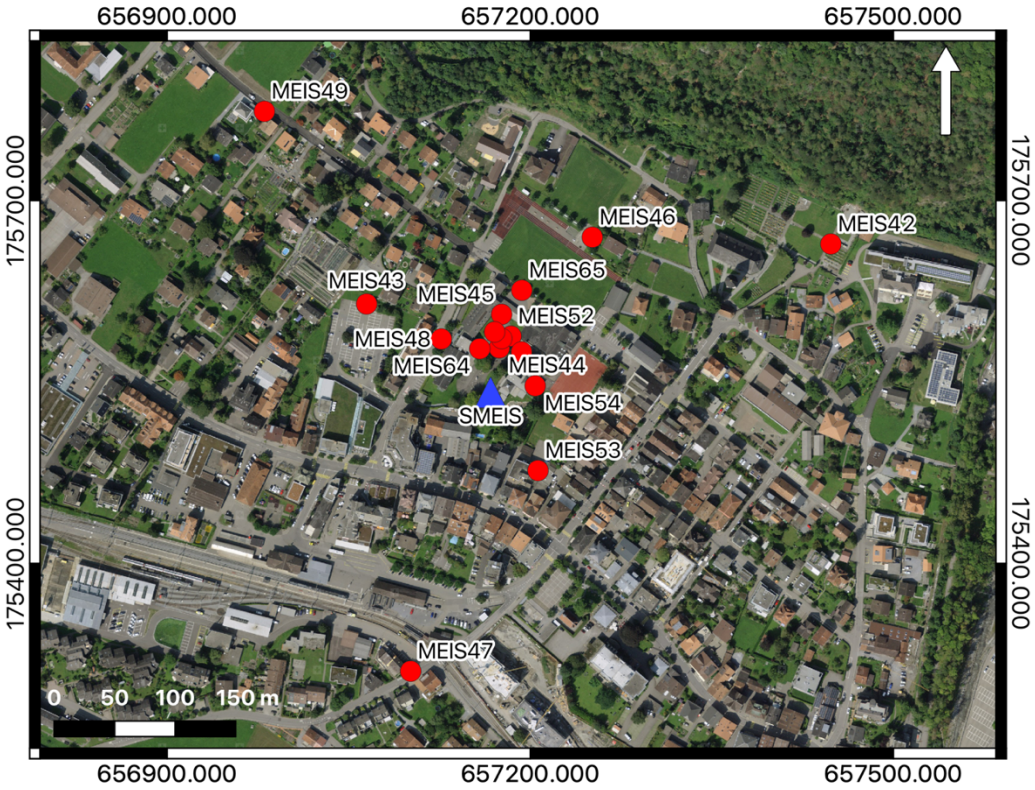

Figure 4: Layout of the array measurement in Meiringen. The locations of the stations for the passive seismic measurement are indicated by the red dots. The blue triangle indicates the seismic station site. Source: Federal Office of Topography.

3.2 H/V and RayDec ellipticity curves

Figure 5 shows the H/V curves determined with the time-frequency analysis method (Fäh et al., 2009) for all stations of the passive array. Most of the H/V curves show a homogeneous trend over the entire frequency range with a similar pattern up to 5.0 Hz. The peak at lower frequency presents a left flank with a low angle, a peak between 1.3 and 1.6 Hz and a steep right flank followed by a well-defined trough. Moving towards south-west and north-east, the frequency of the peak drifts towards lower and higher frequencies, respectively (Fig. 6). For station MEIS49, located northwest of SMEIS1, no peak was detected. The behavior of the H/V curves indicates the presence of a homogeneous layer underneath the central area whose thickness changes only at the extreme borders of our investigated area.

The RayDec technique (Hobiger et al., 2009) is meant to eliminate the contributions of other wave types than Rayleigh waves and give a better estimate of the ellipticity. The RayDec ellipticity curves for all stations of the array measurements are shown in Figure 5 (right plot). These show a pattern similar to the curves obtained through the H/V analysis. In addition to the first peak, a second peak can be clearly recognized at higher frequencies between 10 and 15 Hz.

The dark green curve indicates the array's central station, while the red curve shows the RayDec ellipticity measured at SMEIS1, close to SMEIS.

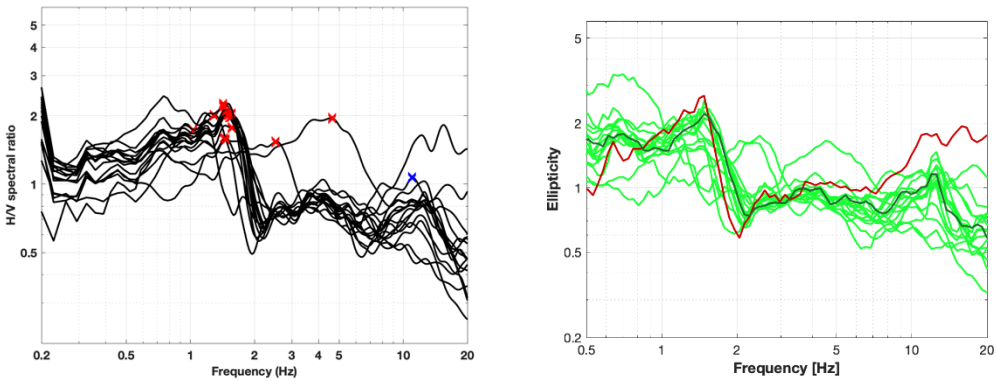

Figure 5: Left: H/V curves of the different stations of the array measurements in Meiringen with picked fundamental frequency (red cross). Right: RayDec ellipticities for all stations of the array. The curve of MEIS55, the array center, is highlighted in dark green, whereas the curve SMEIS1, linked to the measurement nearby the station is highlighted in dark red.

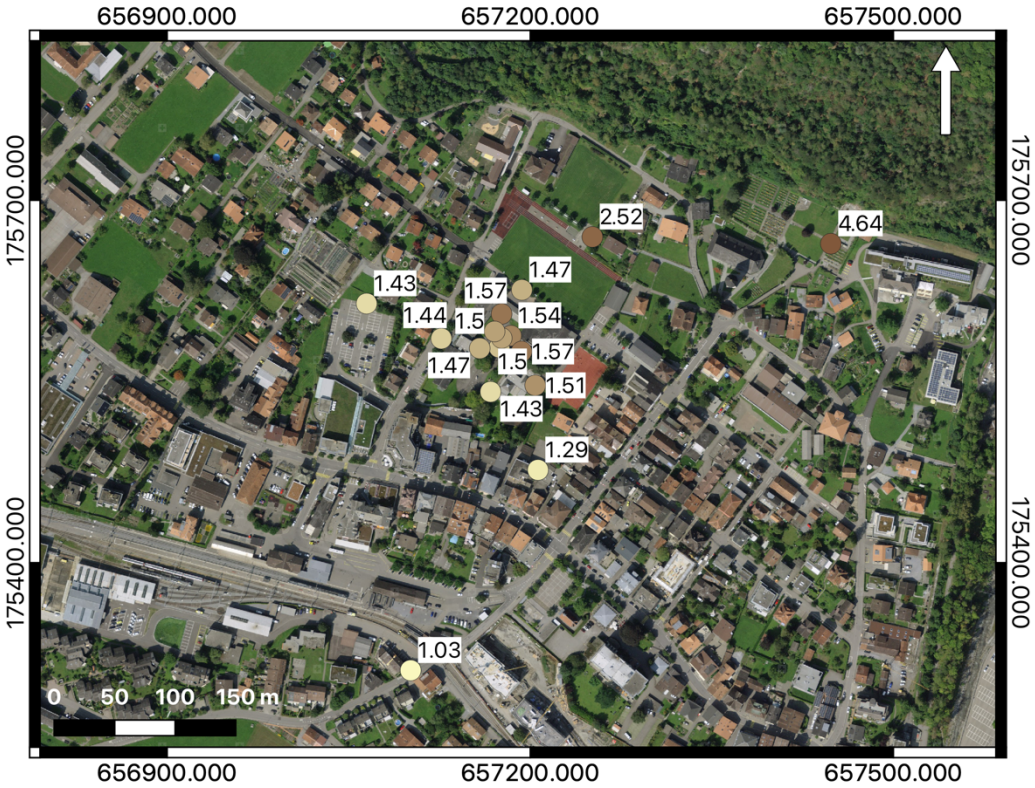

Figure 6: Map showing the variation in frequency for the H/V fundamental peak in the area of Meiringen. Source: Federal Office of Topography.

3.3 Polarization measurements

The polarization analysis was performed according to Burjánek et al. (2010) and Burjánek et al. (2012). The results for all stations of the array are similar. The results for MEIS55, the array center (see location in Fig. 3), are shown in Fig. 7.

The ground motion is slightly linear and horizontally polarized at low frequencies and around the H/V peak (Fig. 7 – left plot); the direction of polarization shown in the right plot (Fig. 7) is northeast-southwest. At other sites, the direction of polarization changes to northwest-southeast in the same frequency range.

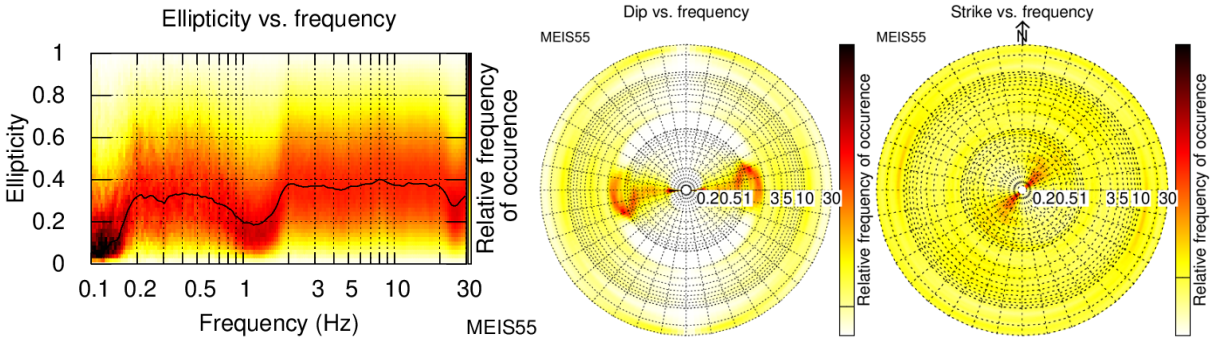

Figure 7: Polarization analysis of station MEIS55.

3.4 3-component high-resolution FK

The results of the 3-component high-resolution FK analysis (Poggi and Fäh, 2010) are shown in Fig. 8. For Love waves, using the transverse component, two dispersion curves were picked, the first one between 1.45 and 27.6 Hz and the second one from 8.0 to 27.7 Hz. A long dispersion curve was also picked for the vertical component between 1.7 and 27.7 Hz. Over the same frequency range, an ellipticity curve gently dipping towards high frequency and with two broad and flat peaks was recognized. Two short curves were picked for the radial component between 2.7 and 10.7 Hz and between 6.4 and 13.5 Hz. The ellipticity curves corresponding to the two picked dispersion curves for the radial component show a wide and asymmetric trough and a peak, respectively.

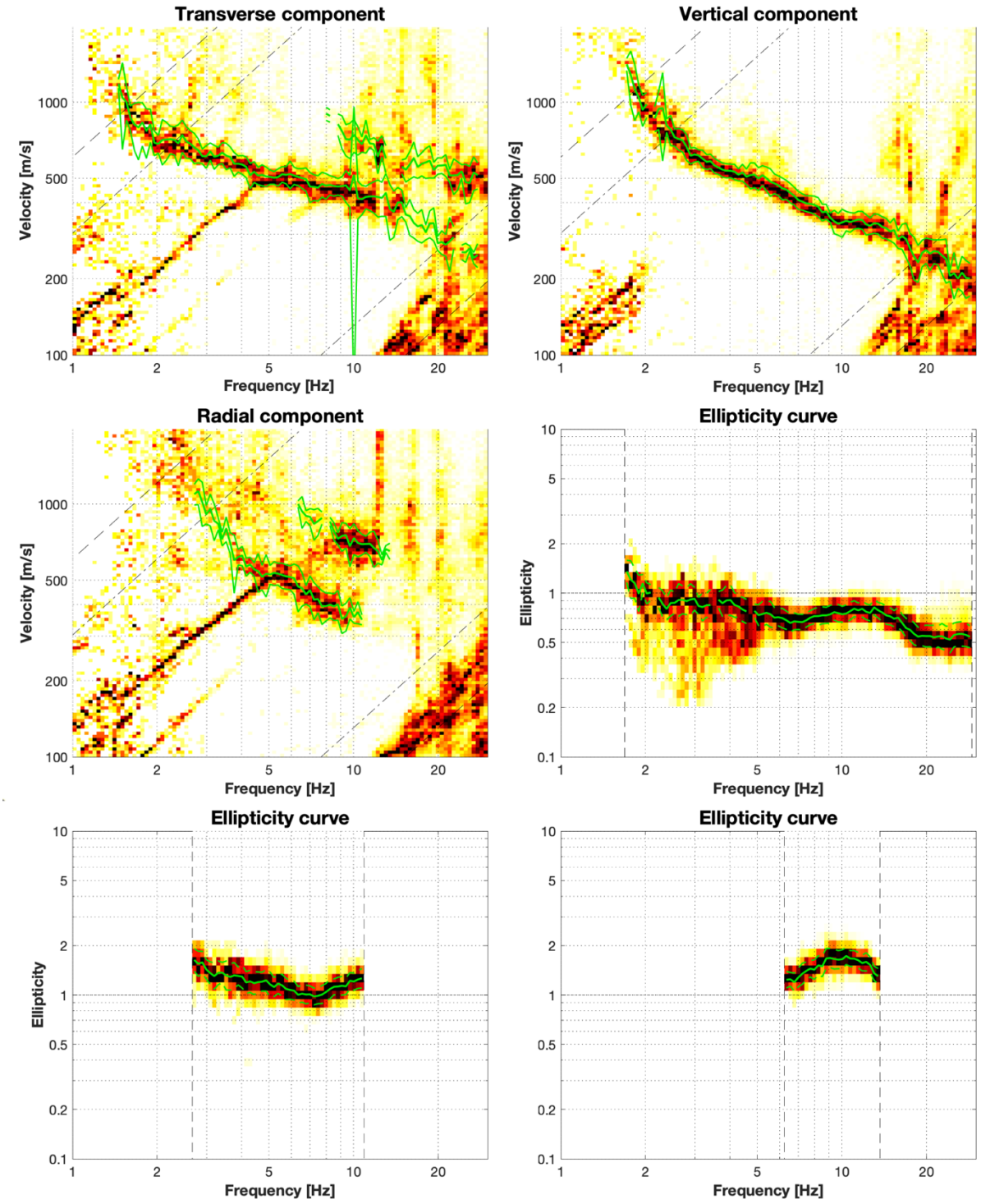

Figure 8: Dispersion curves for the transverse (top row left), radial (top row right) and vertical (middle row left) components and ellipticity curve for the vertical component (middle row right) and radial component (bottom row) obtained with the 3-component HRFK algorithm (Poggi and Fäh, 2010). The dashed and dotted black lines are the array resolution limits. The solid and dashed green lines represent the data picking (central line) and the standard deviation (outer lines).

3.5 WaveDec

The results of the WaveDec (Maranò et al., 2012) processing are shown in Fig. 9. This technique estimates the properties of single or multiple waves simultaneously with a maximum likelihood approach. In order to get good results, the parameter γ must be tuned to modify the sharpness of the wave property estimation between purely maximum likelihood estimation and a Bayesian Information Criterion. Here, a value of $\gamma = 1$ was used, corresponding to a pure Bayesian Information Criterion estimation.

The picking of dispersion curves in WaveDec was performed in the wavenumber-frequency domain. The Love wave dispersion curve was continuously picked between 1.4 and 17.4 Hz. Two Rayleigh wave dispersion curves were picked between 1.9 and 19.1 Hz and between 7.5 and 17.8 Hz. The ellipticity angle for the first mode has negative values between 2.2 and 17 Hz and positive above. For this mode, the particle motion changes from retrograde, where the ellipticity angle is negative, to prograde. At about 2 Hz, the ellipticity angle shows either positive or negative values so that its particle motion is unclear. The ellipticity for the second mode shows a negative ellipticity angle up to 10 Hz and a positive value above. At around 10 Hz, as shown in the bottom right plot, a singularity can be seen. The particle motion is retrograde below 10 Hz and prograde above.

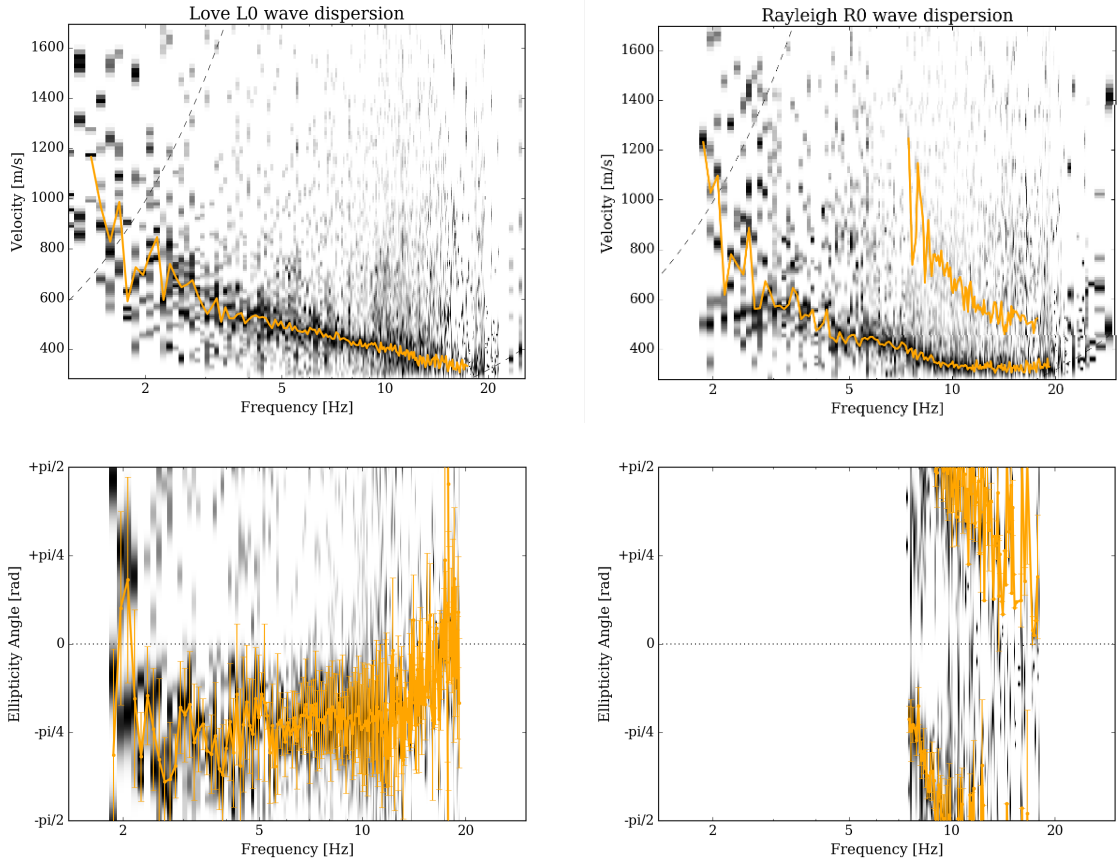

Figure 9: Dispersion curves for Love and Rayleigh waves (top row) and ellipticity angle curves for Rayleigh waves (bottom row) as obtained with WaveDec (Maranò et al., 2012). The dashed black lines (top rows) represent the array resolution limits, the solid orange line indicates the picked curve and the vertical bars at each frequency show the standard deviation for the ellipticity angle curves.

3.6 Modified SPatial AutoCorrelation

The SPAC (Aki, 1957) curves of the vertical components have been calculated using the MSPAC (Bettig et al., 2001) technique implemented in geopsy. Rings with different radius ranges are defined and for all stations pairs with distances inside this radius range, the cross-correlation is calculated in different frequency ranges. These cross-correlation curves are averaged for all station pairs of the respective ring to give the SPAC curves. The rings are defined in such a way that at least three station pairs contribute and that their connecting vectors have a good directional coverage.

The SPAC Autocorrelation curves are shown in Fig. 10 for all selected rings (central and right columns). The black points indicate the data values which contributed to the final dispersion curve estimation, which was picked using the *spac2disp* function of the geopsy. A single dispersion curve was picked for the Rayleigh wave between 1.9 and 11.6 Hz as shown by the dark curve in Fig. 10 (left).

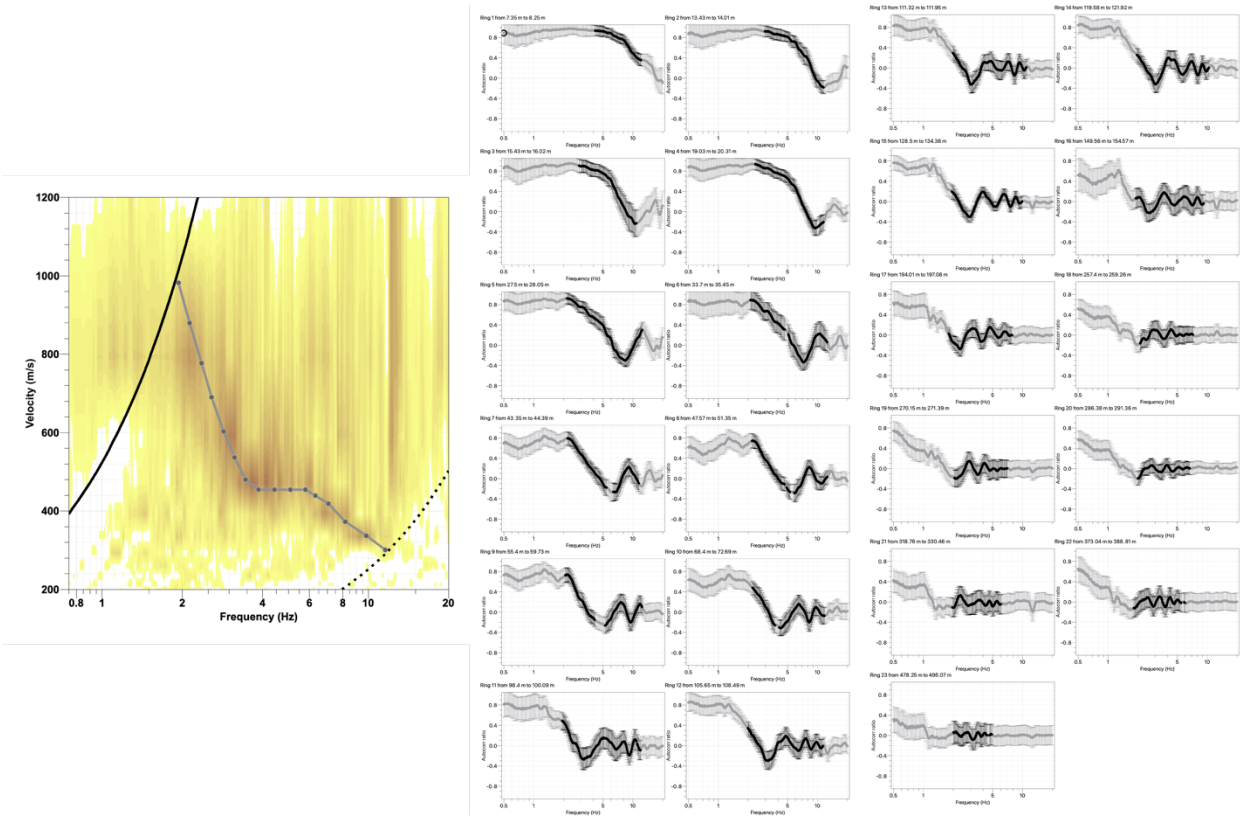

Figure 10: Rayleigh wave dispersion curve (left) obtained using the spac2disp module of geopsy and autocorrelation functions for all rings (center and right). The solid gray line represents the picked data; the black dashed and dotted lines indicate the array resolution limits.

3.7 Summary

Figure 11 gives an overview of the Love and Rayleigh wave dispersion (left and central plots, respectively) and of the Rayleigh wave ellipticity curves (right plot) determined using different approaches. For Love waves, WaveDec produces one dispersion curve, while HRFK provides two dispersion curves. The curve at lower velocity and the curve from WaveDec have similar shape and overlap in the frequency range 1.4-15 Hz. For the Rayleigh waves, the first mode of WaveDec, the first mode of HRFK for the vertical component and the result of MSPAC overlap. The first mode of HRFK for the radial component partially fits the other curves between 4.2 and 10.7 Hz; at lower frequencies, the curve diverges towards higher velocities. The second curves picked for WaveDec and HRFK for the radial component overlap.

The ellipticity curves retrieved using the different methods are quite similar (Fig. 11 - right plot). The RayDec curves refer to the ellipticity for stations MEIS55, the center of the array, and SMEIS1, the station installed close to the permanent station SMEIS. The curves show a similar pattern between 0.8 and 7 Hz with good agreement at the peak and at the trough; at lower and higher frequencies the two RayDec curves diverge.

The WaveDec ellipticities automatically picked after selecting the upper and lower boundaries show a huge scatter both for the first and the second modes. Anyway the shape of the first mode, even if heavily unsmooth, is similar to the RayDec curves. Concerning the results of 3C-HRFK for the vertical component, the curve shows a shape similar to the Raydec curve for the center of the array. The two curves for the radial component, instead, show some similarity with the Raydec curve calculated close to the permanent station.

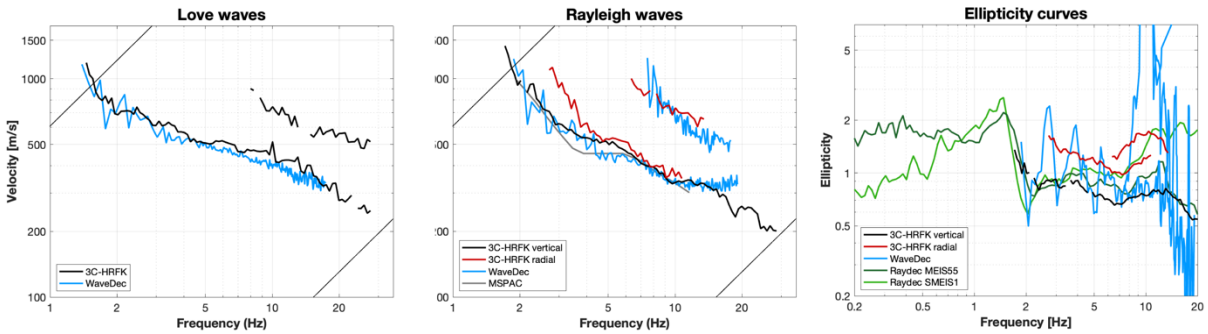

Figure 11: Comparison between the computed Love (left) and Rayleigh (center) wave dispersion curves and ellipticity curves (right).

4 Data inversion

4.1 Inversion targets

We performed several inversions using as much information as possible. The details of the inversion targets are indicated in Table 1 and the corresponding curves are shown in black in Fig. 12.

In the inversion process, we inverted two dispersion curves and the Rayleigh wave ellipticity curve. The dispersion curves, one for the Rayleigh waves and one for the Love waves, were both interpreted as fundamental modes and selected using the results of WaveDec. The RayDec curve measured at SMEIS1, close to station SMEIS, was used as ellipticity curve.

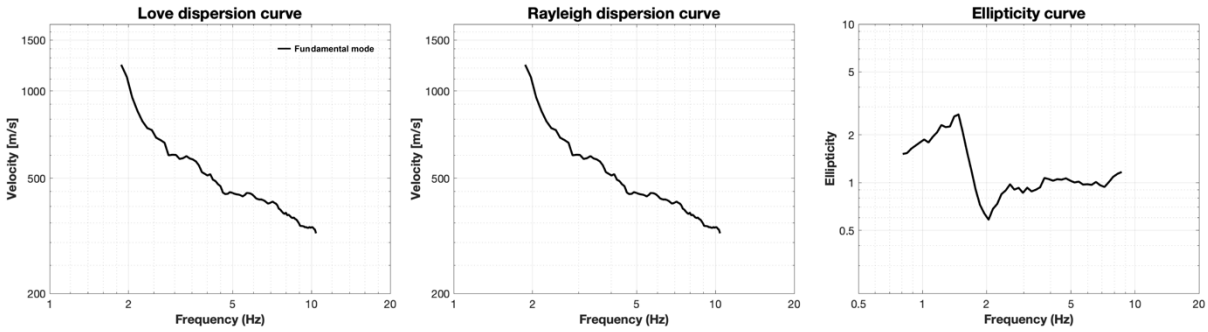

Figure 12: Overview of the dispersion curves used as target for the different inversions.

Additional tests were performed using the second curve picked for the Rayleigh waves using the WaveDec technique. Based on the results obtained, the mode attribution of this curve could be either the first or the second higher mode or a mix of several higher modes. In order to define the correct mode attribution, a further analysis is shown in section 4.5.

Table 1: List of the curves used as target in the inversion.

Method	Wave type	Mode	Curve type	Frequency range [Hz]
WaveDec	Love	fundamental	dispersion	1.4-10.8
WaveDec	Rayleigh	fundamental	dispersion	1.9-10.4
RayDec (SMEIS1)	Rayleigh	fundamental	ellipticity	0.8-8.7

4.2 Inversion parameterization

For the inversion, five different parameterizations were tested. The first four involve free values of thickness and velocities for the different layers, ranging from three to nine layers over the half-space. The S- and P-wave velocities are allowed to range from 50 to 3500 m/s and from 100 to 7500 m/s, respectively. The deepest layer interfaces were allowed to range to a depth of 300 m for all parameterizations. The density was fixed to 2300 kg/m^3 for the bedrock layer and to 2000 kg/m^3 for all the other layers.

The last parametrization had fixed layer thicknesses and consists of 20 layers over the half-space, with the deepest interface at 260 m depth. Equal ranges were defined for the P- and S-wave velocities and density.

4.3 Inversion results

We performed 5 inversions with different parameterizations (see Table 2) using the Dinver routine (http://www.geopsy.org/). Each inversion run produced 280000 models in total in order to assure a good convergence of the solution. The results of these inversions are shown in Figs. 13 – 17.

Table 2: List of inversions

Inversion	Number of layers	Number of models	Minimum misfit
SMEIS 3l	3	280000	0.365
SMEIS 5l	5	280000	0.331
SMEIS 7l	7	280000	0.336
SMEIS 9l	9	280000	0.357
SMEIS fix	20	280000	0.351

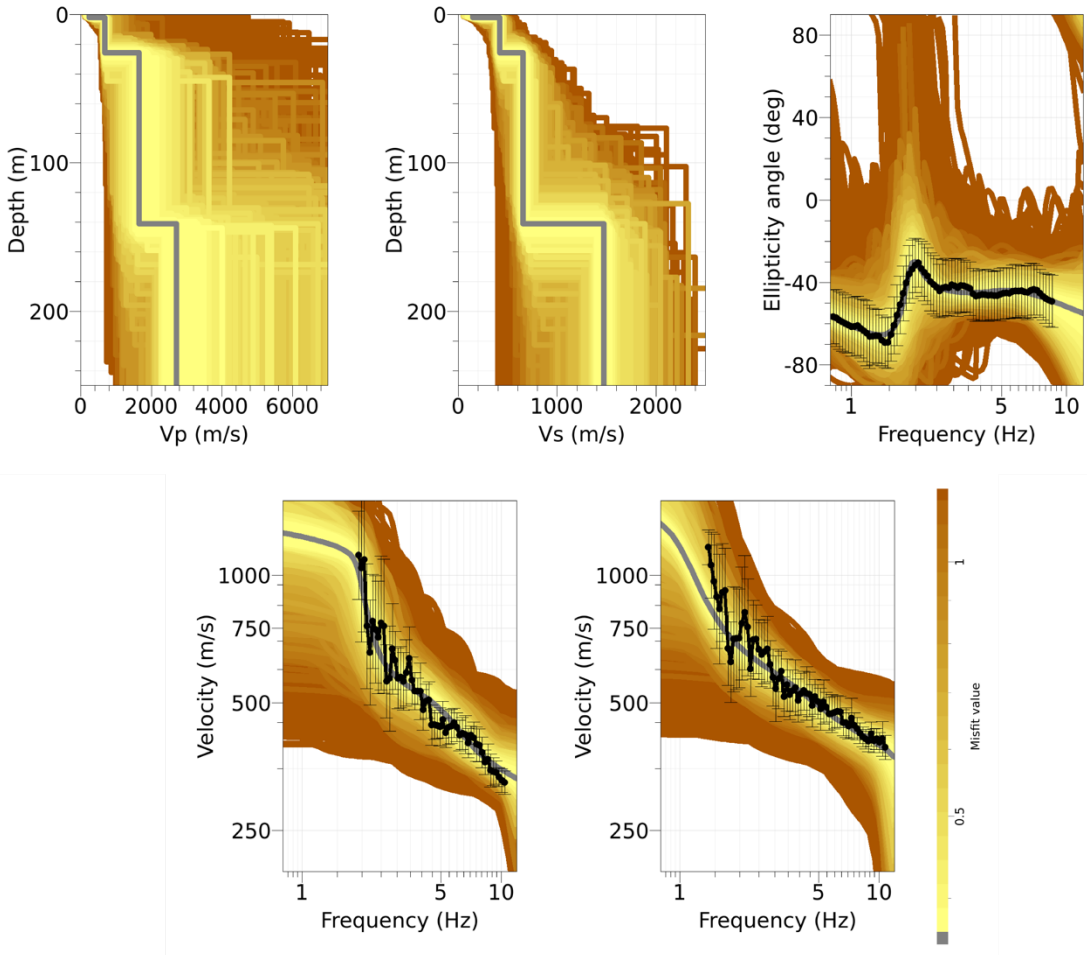

Figure 13: Inversion SMEIS 3l. Top line: P-wave velocity profiles (left), S-wave velocity profiles (center) and Ellipticity angle (right). Bottom line: Dispersion curves for the fundamental mode of Rayleigh (left) and Love (right) waves. The black dots indicate the data points used for the inversion, the black bars the standard deviation of the inverted curve, while the gray line shows the best-fitting model.

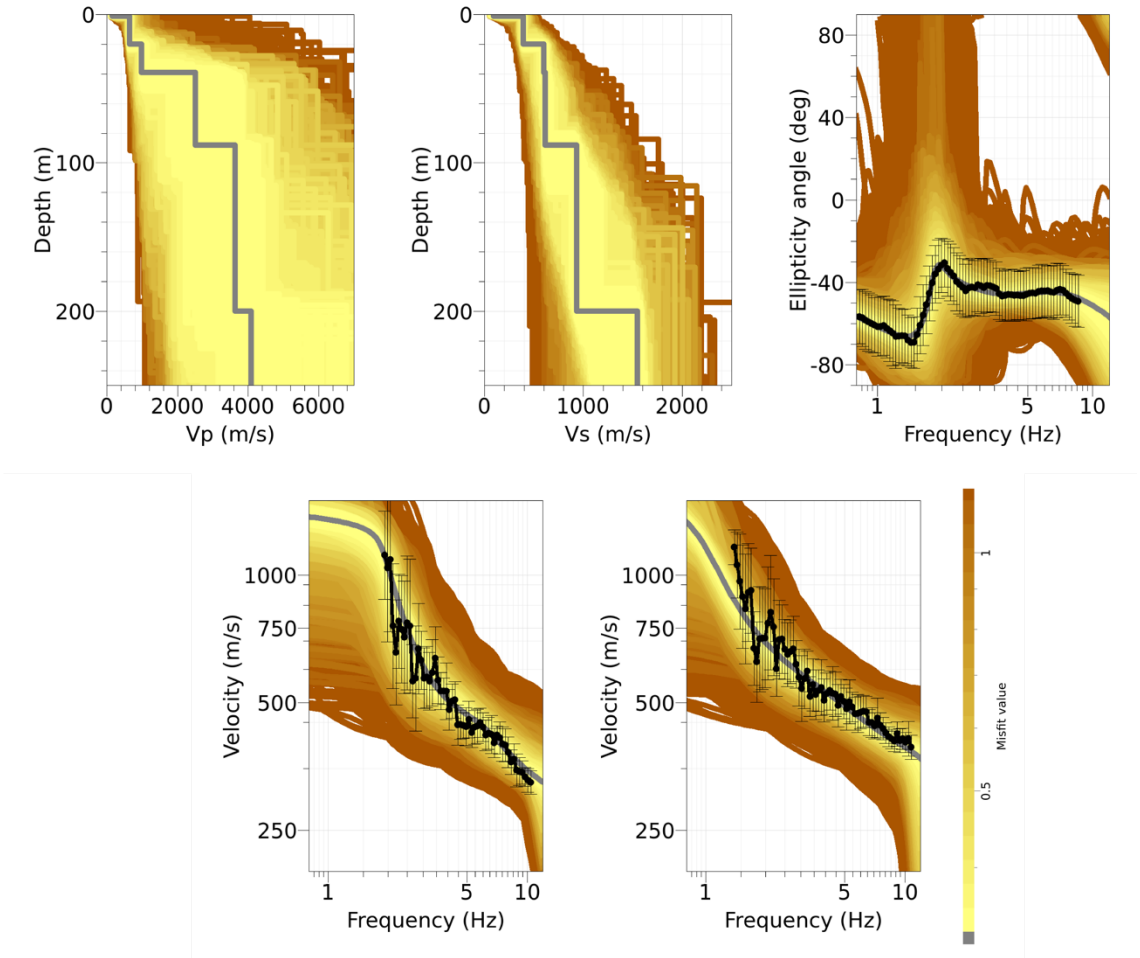

Figure 14: Inversion SMEIS 5l. Top line: P-wave velocity profiles (left), S-wave velocity profiles (center) and Ellipticity angle (right). Bottom line: Dispersion curves for the fundamental mode of Rayleigh (left) and Love (right) waves. The black dots indicate the data points used for the inversion, the black bars the standard deviation of the inverted curve, while the gray line shows the best-fitting model.

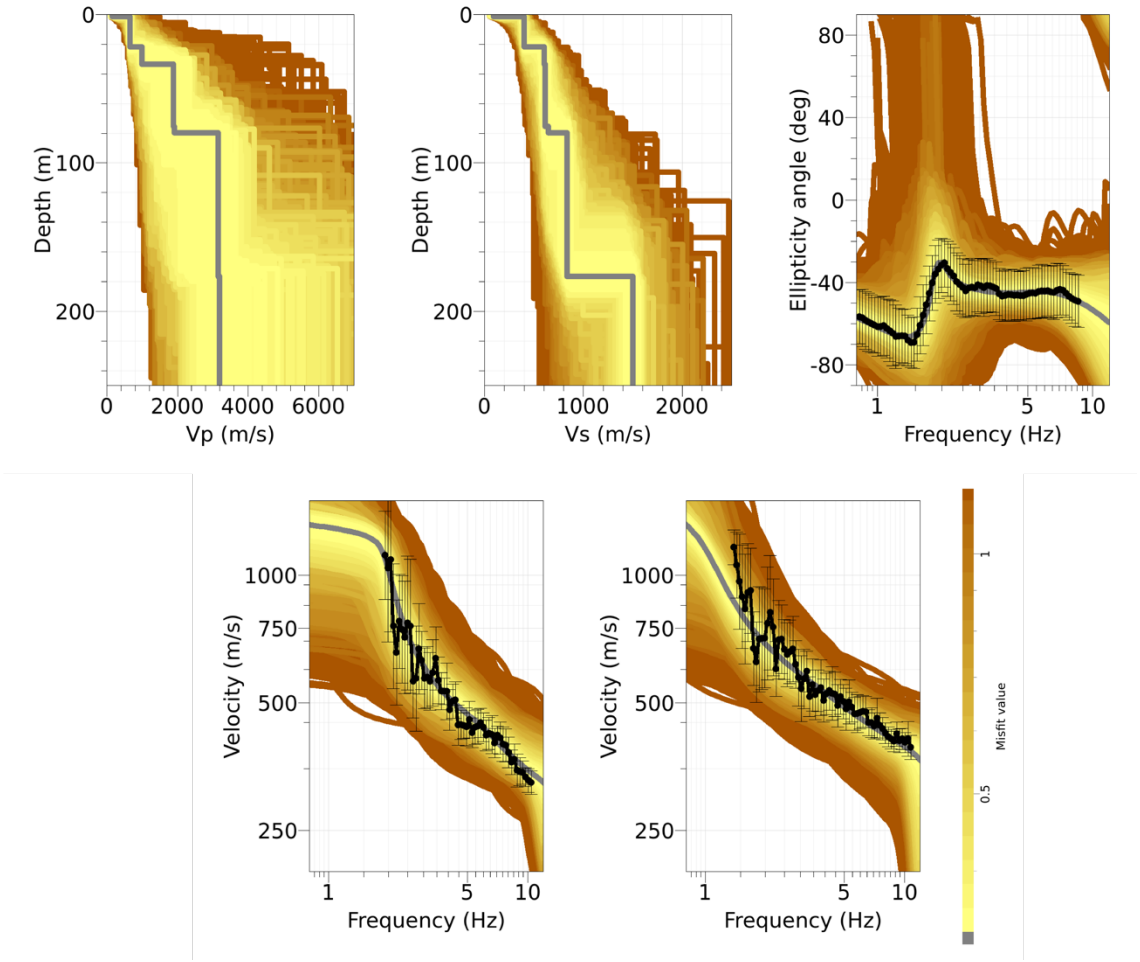

Figure 15: Inversion SMEIS 7l. Top line: P-wave velocity profiles (left), S-wave velocity profiles (center) and Ellipticity angle (right). Bottom line: Dispersion curves for the fundamental mode of Rayleigh (left) and Love (right) waves. The black dots indicate the data points used for the inversion, the black bars the standard deviation of the inverted curve, while the gray line shows the best-fitting model.

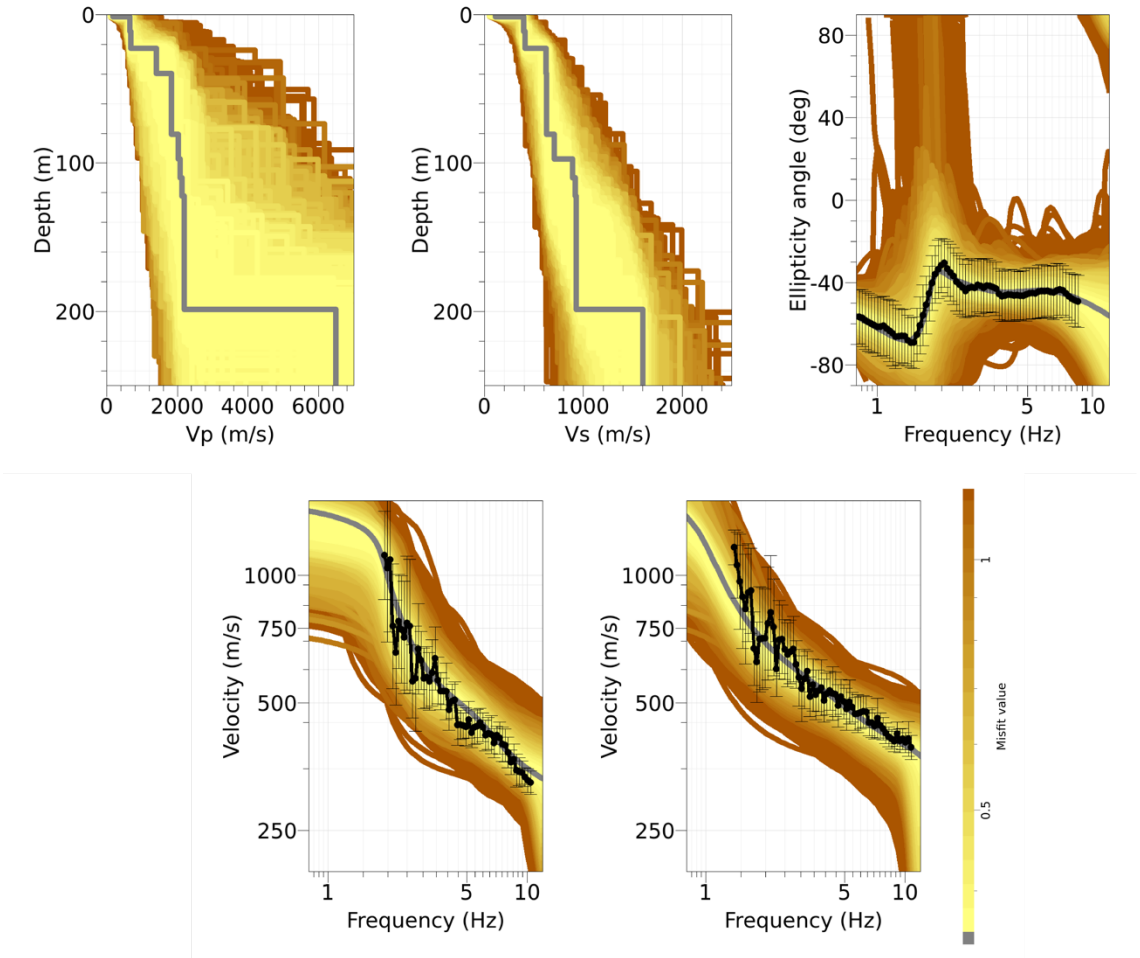

Figure 16: Inversion SMEIS 9l. Top line: P-wave velocity profiles (left), S-wave velocity profiles (center) and Ellipticity angle (right). Bottom line: Dispersion curves for the fundamental mode of Rayleigh (left) and Love (right) waves. The black dots indicate the data points used for the inversion, the black bars the standard deviation of the inverted curve, while the gray line shows the best-fitting model.

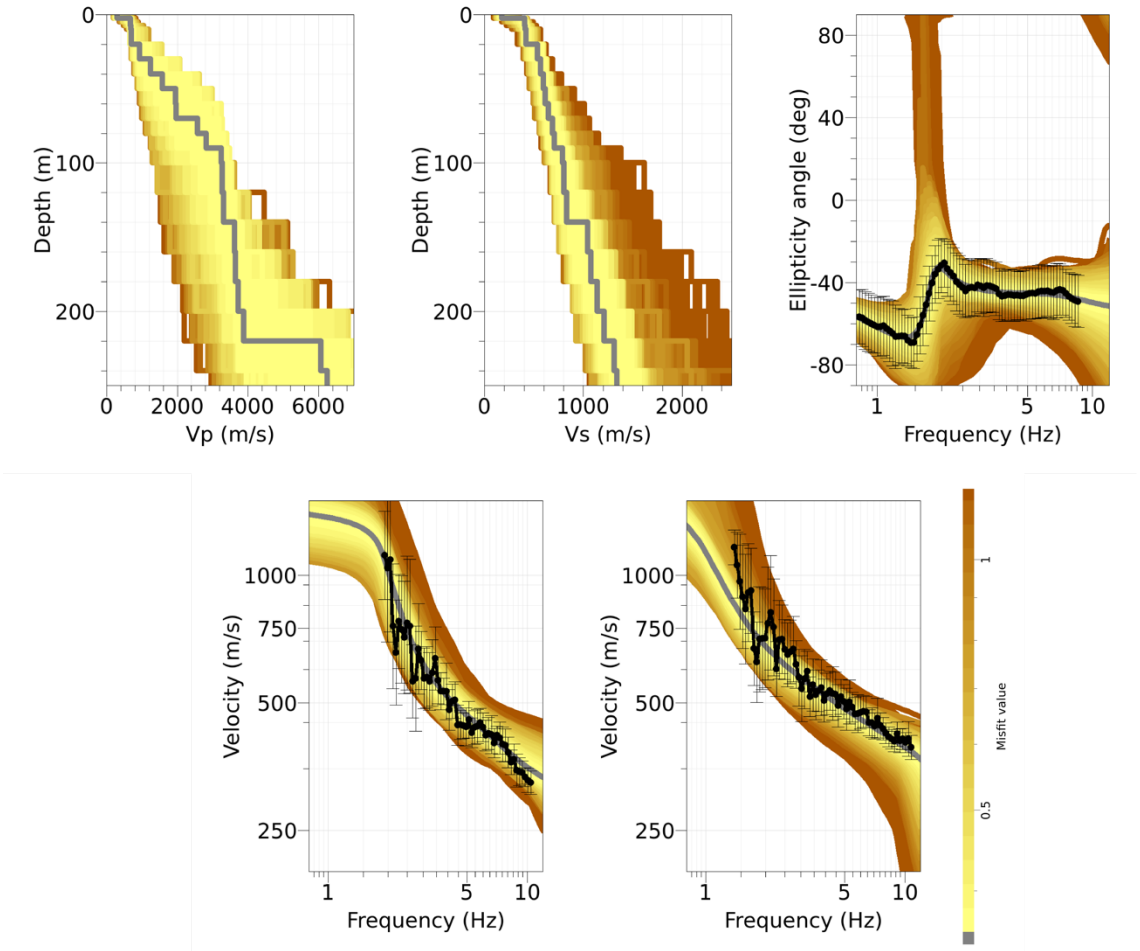

Figure 17: Inversion SMEIS fix. Top line: P-wave velocity profiles (left), S-wave velocity profiles (center) and Ellipticity angle (right). Bottom line: Dispersion curves for the fundamental mode of Rayleigh (left) and Love (right) waves. The black dots indicate the data points used for the inversion, the black bars the standard deviation of the inverted curve, while the gray line shows the best-fitting model.

4.4 Discussion of the inversion results

The best-fitting models from each inversion are shown in Fig. 18.

In the first 30 meters, all velocity profiles show two interfaces: the first at around 1.5 m with S-wave velocity of 400 m/s and the second between 20 and 25 m with S-wave velocities around 600 m/s. A bit deeper, a third interface was recognized at around 90 m by all velocity profiles with the exception of *SMEIS3l.* Consisting of only three layers, it has not enough resolution to fix this interface and the bedrock, therefore finding the half-space at 141 m. The other profiles identify the half-space at 176 m (*SMEIS7l*) and 198 m (*SMEIS5l* and *SMEIS9l*).

The velocity profile obtained using the fixed layer parametrization (*SMEIS fix*) shows a constant increase of velocity with depth. This profile reproduces the two shallow interfaces at 1.5 and 20 meters. The third interface and the transition to the half-space are also in agreement with the other profiles in terms of depth but do not show any major velocity contrast.

The velocity profiles resulting from the different inversions have V_{S30} between 380.2 and 406.4 m/s, with an average value of 388.4 ± 10.5 m/s.

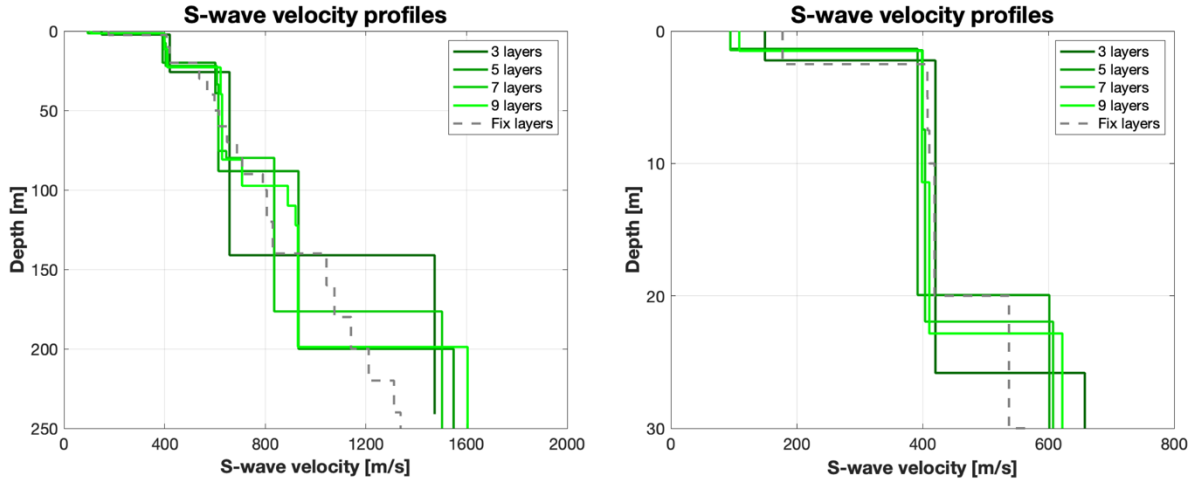

Figure 18: Overview of the best shear-wave velocity profiles of the different inversions (left) and zoom on the upper 30 m of the inversion profiles.

4.5 Forward modeling

After having defined the best parametrization for the investigated area using the fundamental modes of Rayleigh and Love waves and the ellipticity angle of Rayleigh waves, the synthetic dispersion curves were computed using the best velocity profile of *SMEIS 9l* is shown in Figure 16 (grey profile). As expected by the good fit during the inversion, the synthetic dispersion curves fit the fundamental mode of Rayleigh and Love waves. The curves interpreted as higher modes for the Love and Rayleigh waves, instead, consist in a mix of several modes, as shown by the synthetic dispersion curves in ochre color (Fig. 19) and a definitive mode attribution is not possible.

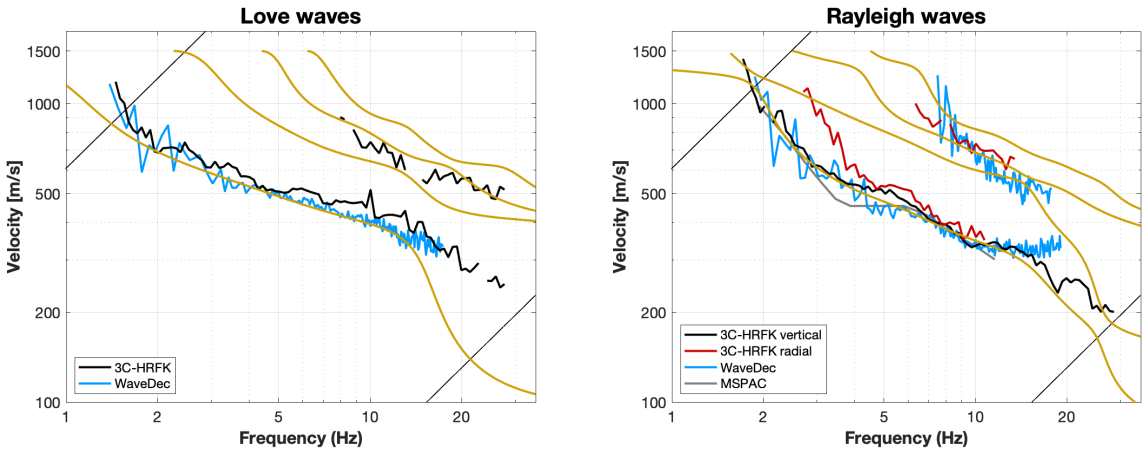

Figure 19: Comparison between the computed Love (left) and Rayleigh (right) wave dispersion curves. The ochre curves correspond to the synthetic dispersion curves computed using the velocity profile with the lowest misfit from the inversion in Fig. 15.

5 Further results from the inverted profiles

5.1 SH transfer function

In Figure 20, the average theoretical shear-wave transfer function for the best model of *SMEIS5l*, *SMEIS7l*, *SMEIS9l* and *SMEIS fix* and the empirical amplification at station SMEIS are shown. For the investigated site, the models predict an amplification included between 1.4 and 3.8 in the frequency range 0.8 – 12 Hz with several peaks. Above 10 Hz, the SH transfer function shows a wide peak with amplification values up to 8 at about 17.5 Hz. The present (10.03.2021) empirical amplification has a maximum of 30 earthquakes between 0.8 and 6.3 Hz decreasing to 1 above 26 Hz. Even if the number of recorded earthquakes is low, similar shapes can be recognized between the two curves. The wide peak in the SH transfer function is shifted towards higher frequencies and higher amplification values if compared to the same peak in the empirical amplification at station SMEIS.

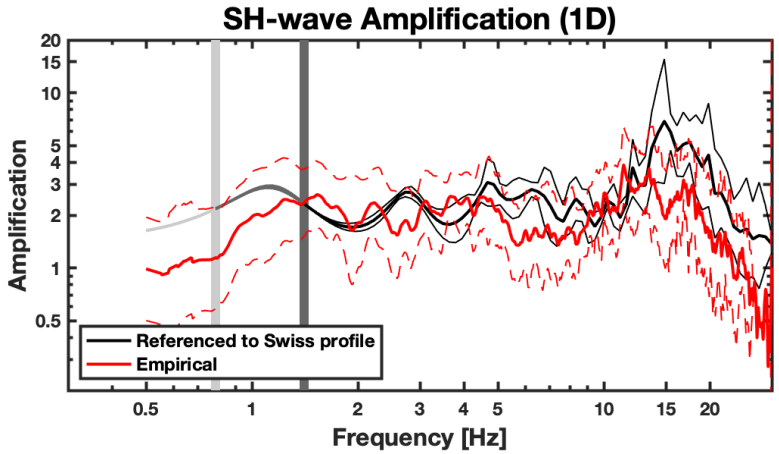

Figure 20: Modeled amplification function and standard deviation (black lines). Red curves represent the empirical amplification (solid line) and its standard deviation (dashed lines) function at station SMEIS.

5.2 Quarter-wavelength representation

The quarter-wavelength velocity approach (Joyner et al., 1981) provides, for a given frequency, the average velocity at a depth corresponding to 1/4 of the wavelength of interest. Figure 21 shows the quarter-wavelength results for the inversion of Figure 16 using the fundamental modes of Rayleigh and Love wave dispersion curves and the Rayleigh wave ellipticity angle. The results using this proxy, considering frequency limits of the experimental data between 1.4 to 10.8 Hz for the dispersion curves and between 0.8 and 8.7 Hz for the ellipticity curves, is well constrained down to 30 m and below. The quarter-wavelength impedance contrast introduced by Poggi et al. (2012) is also displayed in the figure. It corresponds to the ratio between two quarter-wavelength average velocities, respectively from the top and the bottom part of the velocity profile, at a given frequency.

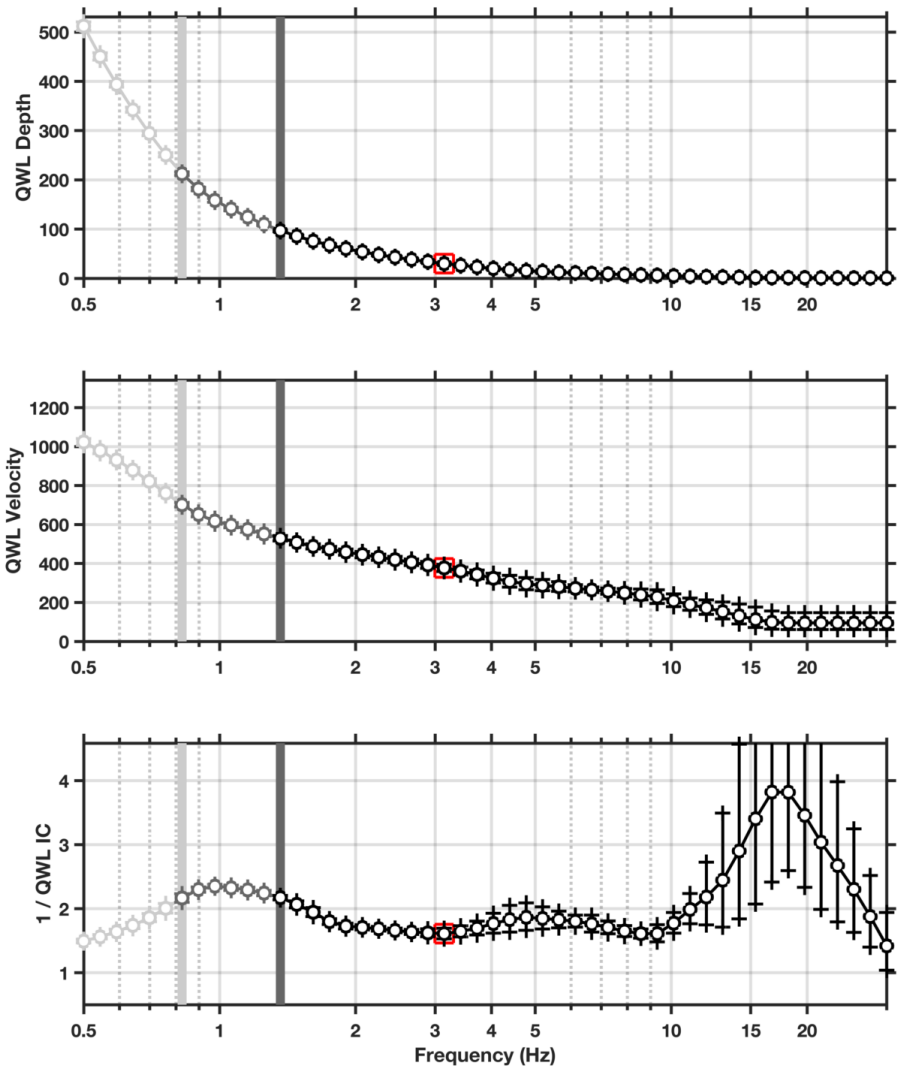

Figure 21: Quarter wavelength representation of the velocity profiles for the best models of the inversions (top: depth, center: velocity, bottom: impedance contrast). The light grey bar shows the lowest ellipticity frequency value, the dark grey bar indicates the lowest frequency value obtained with dispersion curves and the red square corresponds to f_{30} (frequency related to the depth of 30 m).

6 Discussion and conclusions

The passive array measurement performed in Meiringen in September 2020 allowed the investigation of the subsurface beneath station SMEIS.
The H/V analysis pointed out that the center of the study area consists in a homogeneous layer dipping towards northeast. A second peak at about 15 Hz, not clearly visible in the H/V curves, can be recognized using the RayDec curves (Fig. 5 – right plot).

The inversion of Rayleigh and Love wave dispersion curves and of the Rayleigh ellipticity curve yields P- and S-wave velocity profiles investigating the subsurface down to about 250 m. All velocity profiles show two shallow interfaces at 1.5 and 20-25 meters. The third main interface is identified by the velocity profiles with 5, 7 and 9 layers. The 3-layer profile, due to its low resolution, is not able to represent the deep subsurface, pushing the depth of the half-space to 141 m. The bedrock was estimated at 176 m by the model with 7 layers and at 198 by the *SMEIS5l* and *SMEIS9l* models.
The velocity profile obtained using the fix-layer parametrization *(SMEIS fix*) shows a gradual increase of the velocity without strong interfaces. The V_{S30} value of the site is 380 m/s, corresponding to soil class B in EC8 and C in SIA261 classifications.
The theoretical shear-wave transfer function predicts an amplification of around 2 between 0.8 and 10 Hz followed by a peak at around 17.5 Hz with an amplification factor equal to 8. The comparison was also made with amplification observations at this station, showing a quite good agreement in the flat portion and slight shift towards higher values at the peak.

References

Burjánek, J., Gassner-Stamm, G., Poggi, V., Moore, J. R., and Fäh, D. (2010). Ambient vibration analysis of an unstable mountain slope. Geophys. J. Int., 180:820–828.

Burjánek, J., Moore, J. R., Molina, F. X. Y., and Fäh, D. (2012). Instrumental evidence of normal mode rock slope vibration. Geophys. J. Int., 188:559–569.

Fäh, D., Gardini, D., et al. (2003). Earthquake Cataloque of Switzerland (ECOS) and the related macroseismic database. Eclogae geol. Helv. 96.

Fäh, D., Wathelet, M., Kristekova, M., Havenith, H., Endrun, B., Stamm, G., Poggi, V., Burjanek, J., and Cornou, C. (2009). Using ellipticity information for site characterisation. NERIES deliverable JRA4 D4, available at http://www.neries-eu.org.

Fritsche, S., Fäh, D., Gisler, M., and Giardini, D. (2006). Reconstructing the damage field of the 1855 earthquake inSwitzerland: historical investigations on a well-documented event Geophys. J. Int. (2006)166, 719–731

Hobiger, M., Bard, P.-Y., Cornou, C., and Le Bihan, N. (2009). Single station determination of Rayleigh wave ellipticity by using the random decrement technique (RayDec). Geophys. Res. Lett., 36.

Maranò, S., Reller, C., Loeliger, H.-A., and Fäh, D. (2012). Seismic waves estimation and wavefield decomposition: Application to ambient vibrations. Geophys. J. Int., 191:175–188.

Poggi, V. and Fäh, D. (2010). Estimating Rayleigh wave particle motion from three component array analysis of ambient vibrations. Geophys. J. Int., 180:251–267.

Poggi, V., Edwards, B., and Fäh, D. (2010). Characterizing the Vertical-to-Horizontal Ratio of Ground Motion at Soft-Sediment Sites. Bulletin of the Seismological Society of America, 102(6): 2741 2756.